JCB Journal of Cell Biology

ARTICLE

Signal strength controls the rate of polarization within CTLs during killing

Gordon L. Frazer, Christian M. Gawden-Bone, Nele M.G. Dieckmann, Yukako Asano, and Gillian M. Griffiths

Cytotoxic T lymphocytes (CTLs) are key effector cells in the immune response against viruses and cancers, killing targets with high precision. Target cell recognition by CTL triggers rapid polarization of intracellular organelles toward the synapse formed with the target cell, delivering cytolytic granules to the immune synapse. Single amino acid changes within peptides binding MHC class I (pMHCs) are sufficient to modulate the degree of killing, but exactly how this impacts the choreography of centrosome polarization and granule delivery to the target cell remains poorly characterized. Here we use 4D imaging and find that the pathways orchestrating killing within CTL are conserved irrespective of the signal strength. However, the rate of initiation along these pathways varies with signal strength. We find that increased strength of signal leads to an increased proportion of CTLs with prolonged dwell times, initial Ca^{2+} fluxes, centrosome docking, and granule polarization. Hence, TCR signal strength modulates the rate but not organization of effector CTL responses.

Introduction

Cytotoxic T lymphocytes (CTLs) are key effector cells in the immune system, killing targets with high precision. This is achieved through the specificity of the clonally expressed T cell receptor (TCR) for a specific peptide presented by major histocompatibility complex I (pMHC). TCR–pMHC binding triggers signaling and induces the CTL to polarize and dock the centrosome at the point of TCR signaling, allowing precise delivery of cytotoxic granules. Recent studies have demonstrated that TCR signals modulate membrane changes and reorganization of the actin cytoskeleton at the point of secretion (Gawden-Bone et al., 2018; Ritter et al., 2015; Ritter et al., 2017). However, little is known about how the many steps required for intracellular polarization of the secretory machinery within CTL change with the strength of TCR signal.

The Ova-tcr-I (OTI) transgenic mouse provides a particularly well-understood system for examining the effects of altering the strength of TCR signaling. All T cells in OTI transgenic mice express a clonal TCR recognizing peptides from ovalbumin, with the canonical peptide that binds MHCI ($H2K^b$) being SIINFEKL (OVA257-264; Hogquist et al., 1994; Kelly et al., 1993; Koniaras et al., 1999). Single amino acid changes in this peptide, termed altered peptide ligands (APLs), have been used to alter CTL killing within a population of cells. This OTI system is exceptionally well-described, with the strength of pMHC–TCR interactions understood at the structural level (Denton et al., 2011) via studies describing the binding rates and strength of TCR–pMHC interactions for different APLs (Alam et al., 1996; Alam et al., 1999; Naeher et al., 2007; Huang et al., 2010; Liu et al., 2014). The impact of varying strength of interactions upon CTL activation (King et al., 2012; Naeher et al., 2007; Ozga et al., 2016; Palmer et al., 2016; Zehn et al., 2009; Zehn et al., 2014) and killing efficiency is also well-characterized within CTL populations (Daniels et al., 2006; Hogquist et al., 1995; Hogquist et al., 1994; King et al., 2012; Ozga et al., 2016; Zehn et al., 2009). Previous studies using this system have shown a reduction in the number of conjugates formed between CTLs and targets (Jenkins et al., 2009; Palmer et al., 2016; Yachi et al., 2006), and suggested that granule polarization was reduced with lower-affinity ligands (Jenkins et al., 2009). However, these studies examined a snapshot of events within a population of cells at fixed time points. Little is known about how varying strength of TCR signaling controls the polarization and delivery of killing within individual CTLs within the population.

Several possible mechanisms exist by which stimulation strength might affect killing. First, the coordination of each of the different stages required for successful killing (attachment, centrosome, and granule polarization) could change with signal strength; for example, centrosome polarization to the synapse might occur without concomitant granule polarization (Beal et al., 2009; Jenkins et al., 2009). Conversely, the speed of individual stages within the process might change; for example, the speed of centrosome movement might be dictated by

Cambridge Institute for Medical Research, Biomedical Campus, Cambridge, UK.

Correspondence to Gillian M. Griffiths: gg305@cam.ac.uk.

strength of signal. Alternatively, the coordination of individual steps might be modulated in rate but not organization by stimulation strength, as was previously observed during activation of naive T cells (Ma et al., 2020; Richard et al., 2018). Here we use high-resolution 3D and 4D spinning-disk confocal microscopy and image analysis to interrogate the stages of CTL killing and hence distinguish these possibilities, revealing how CTL killing efficiency is controlled.

Results

Increasing TCR signal strength increases the time CTLs dwell on a target

We used a lactate dehydrogenase (LDH) release assay to measure target cell death. Consistent with previous studies, we found that increasing TCR signal strength by varying APL to increase TCR–pMHC affinity resulted in increased killing (Daniels et al., 2006; Fig. S1 a). This increase in killing efficiency mirrored the increase in CTL degranulation (Fig. S1, b–d).

To establish how signals of increasing strength increased killing, we first investigated how signal strength affected the length and number of contacts between CTLs and target cells. Using spinning-disk microscopy to image live CTLs interacting with targets in 3D (4D imaging), we found a significant increase in dwell time with higher-affinity ligands (Fig. 1, a and b; and Video 1). Furthermore, as TCR signal strength was increased, the mean number of CTL target interactions per CTL decreased, with a mean ± SD of 5.63 ± 4.75 interactions per CTL for targets pulsed with the weakest APL (G4) over 40 min to 4.77 ± 3.61 for T4 (mid), and only 4.03 ± 2.66 for N4 (strong; Fig. 1 c). These data indicate that CTL–target cell interactions stimulated by higher-affinity ligands give rise to a more homogeneous response, with CTLs contacting fewer targets for longer times.

Loss of charge and the resulting depletion of actin from the synapse are impaired with weak TCR signaling

Previous studies have shown that actin controls granule release at the cytolytic synapse, with phosphatidylinositol 4,5-bisphosphate (PIP2) required for actin recruitment across the synapse (Ritter et al., 2017). Upon TCR signaling, PIP2 is rapidly cleaved to generate diacylglycerol. This results in the loss of actin recruitment and changes the charge across the membrane, preventing phosphatidylinositol-4-phosphate 5-kinase association required to replace PIP2 (Gawden-Bone et al., 2018). To examine if TCR signal strength modulates the loss of negative charge and depletion of actin from the synapse, we used OTI CTLs nucleofected with an EGFP-Kras8^{+} probe to detect membrane negative charge, along with phalloidin (F-actin) and anti-phospho-tyrosine to identify synapses where signaling had occurred in fixed conjugates. Using en face image analysis and quantitation, we found a greater depletion of both membrane charge and actin across the synapse in conjugates formed with strong- (N4) compared with weak- (G4) affinity ligands (Fig. 2). The mean area of both charge and actin depletion increased with the higher-affinity ligand (N4) compared with the weak ligand (G4; Fig. 2, e and f). These depletions showed similar results with conjugates formed for 15 or 30 min. Thus, stronger TCR signals resulted in an increased frequency of long-term interactions between CTLs and targets. In addition, stronger signals promoted an increased proportion of CTLs depleting actin across the synapse, in keeping with the molecular mechanism of actin depletion proposed (Gawden-Bone et al., 2018). As increased dwell times are likely to result in sustained signaling, it is possible that these two changes work in concert.

Increasing TCR signal strength enhances centrosome polarization to the synapse

Polarization of the centrosome to the synapse plays a crucial role in directing degranulation of cytolytic components toward the target cell. We used the pericentrin-AKAP450 centrosomal targeting (PACT) domain (Gillingham and Munro, 2000) to follow centrosome polarization to the synapse as CTLs formed conjugates with targets (Fig. 3 and Video 2). Tracking the centrosome within individual CTLs that formed a stable conjugate with a target cell, we found that with N4 stimulation, the centrosome traversed the cell to dock at the synapse (defined as <1 µm from the synapse) within 600 s in 80% of conjugates, and the centrosome had docked in 100% of conjugates by 750 s. In contrast, the centrosome docked in only 55% of conjugates by 600 s for T4, with only 66% docking by 750 s. In response to G4 stimulation, centrosome docking was only seen in 20% of conjugates by 600 s, increasing to 30% by 750 s. Of note, at 900 s, the centrosome was docked in 60% of conjugates for N4, 33% for T4, and 0% for G4 (Fig. 3, a and b). This suggests that with higher-affinity ligands, the frequency of cells with docked centrosomes at the synapse increases with TCR signal strength.

We next asked whether the speed of centrosome movement varied, but found no substantial differences in the timing or maximum speed with which centrosomes docked at the synapses when stimulated by N4, T4, or G4 pMHC interactions (Fig. S2). Fluctuations were observed post-docking after stimulation with G4, in keeping with the variations in centrosome distance from the synapse observed with G4 that suggest docking was transient and less stable with weaker signals (Fig. 3 b). Thus, the speed of centrosome movement appeared constant, but the frequency of CTLs with docked centrosomes increased with TCR signal strength.

We verified this by measuring the closest centrosome distance to the synapse in 3D live imaging of a population of CTLs interacting with targets over a 40-min period, including transient interactions (Fig. 3 c). We found that centrosome docking occurred in some CTLs regardless of stimulation strength, albeit only transiently with weaker signals. Only when an irrelevant peptide (NP68) was used was no docking seen. Thus, while centrosome docking occurred regardless of signal strength, the rate at which centrosome docking was achieved within the CTL population varied according to signal strength.

Docking of the centrosome promotes simultaneous delivery of granules to the synapse

Previous work investigating the impact of APL on centrosome and granule polarization in fixed conjugates suggested that lower signal strength led to centrosome but not granule polarization to the synapse (Jenkins et al., 2009). We therefore

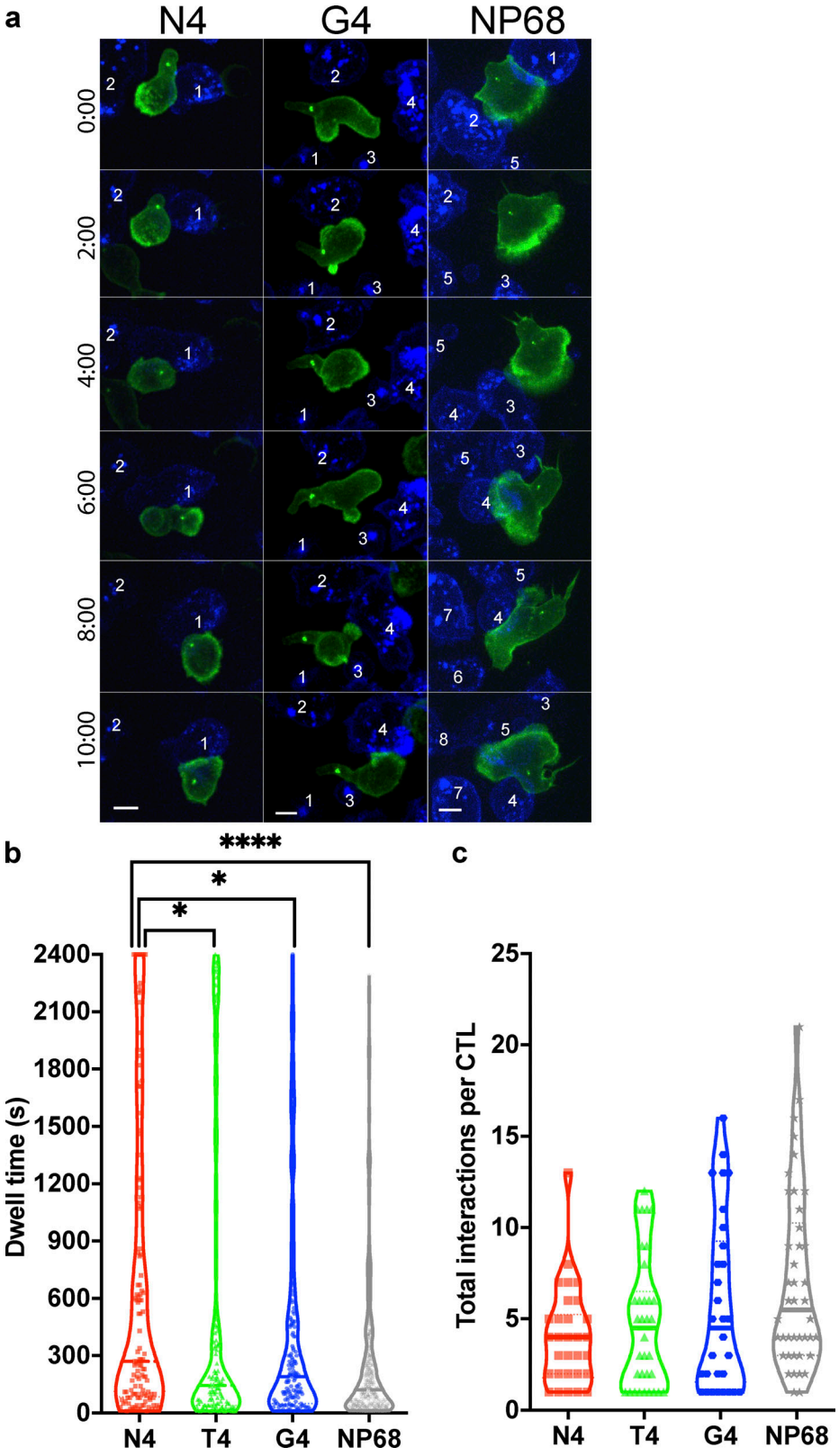

Figure 1. **Increasing TCR signal strength increases CTL dwell time. (a)** OTI CTLs expressing Lifeact-mApple (green) and RFP-PACT (green sphere) interacting with EL4 (blue), pulsed with N4, T4, G4, or NP68 peptides. Representative time series of OTI CTLs encountering targets, numbered sequentially. Scale bars = 5 µm. **(b)** Violin plot showing dwell times for individual CTLs with targets; number of interactions N4 *n* = 121, T4 *n* = 128, G4 *n* = 169, NP68 *n* = 294; bars represent median with quartiles. A Bonferroni-corrected Mann–Whitney test was used for statistical analysis. *, P < 0.5; ****, P < 0.0001. **(c)** Data from (b) were used to calculate the mean number of interactions per CTL per time series and plot the mean per independent video (N4 *n* = 30, T4 *n* = 34, G4 *n* = 30, NP68 *n* = 42). Bars represent median with quartiles.

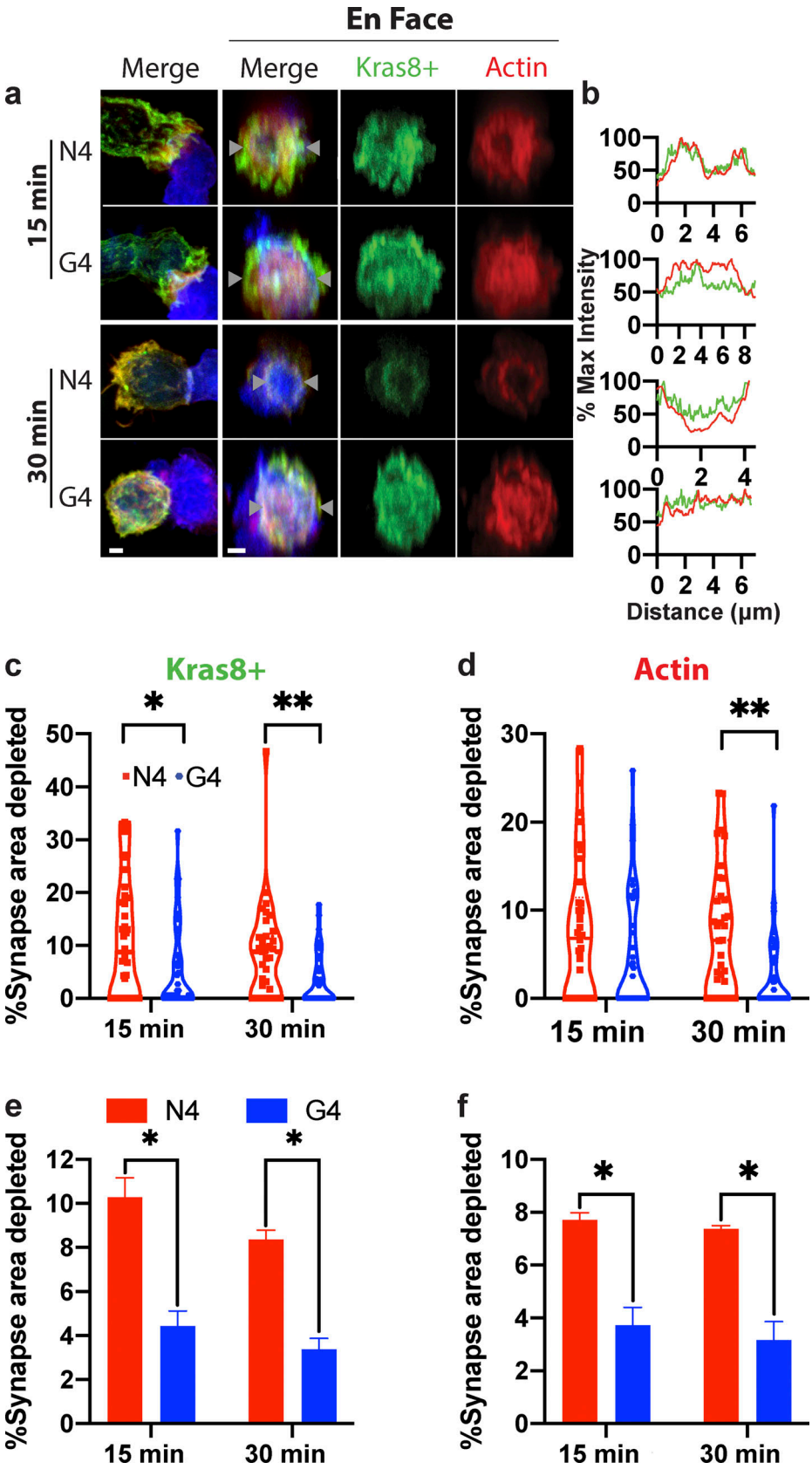

Figure 2. **Increasing TCR signal strength increases actin depletion.** Confocal projections showing cell conjugates or 3-μm depth en face reconstructions across the synapse for OTI CTLs expressing Kras8⁺ probe (green) conjugated with N4 or G4 presenting EL4 for times as shown before fixation and labeling for actin (red). **(a)** Representative images of conjugates showing actin (red), Kras8⁺ in (green), and EL4 (blue). Maximum intensity projections (left) and en face

projections (right) for merged, actin, and Kras8$^+$ signals. Scale bars = 1 µm. **(b)** Intensity profiles for actin and Kras8$^+$ along line marked between gray triangles. **(c and e)** Area of synapse depleted for Kras8$^+$ expressed as a percentage of the total synapse area taken from the en face images for each individual cell in one representative experiment (c; *n* = 30 per condition) and the mean (e); bars show SEM from three separate repeats. **(d and f)** Area of synapse depleted for actin as a percentage of the total synapse area taken from the en face images for each individual cell in one representative experiment (d; *n* = 30 per condition) and the mean (f); bars show SEM from three separate repeats. A two-tailed Bonferroni-corrected Mann–Whitney test was used for statistical analysis of c–f. *, P < 0.5; **, P < 0.01.

followed the polarization of the centrosome and granules using 4D imaging (Fig. 4 and Video 3). To determine if clustering of granules around the centrosome was impaired with weak TCR signal strength, we measured the distance from each granule to the centrosome as they polarized toward the synapse (Fig. 4, a–c). We found that with strong signals granules behaved similarly to each other, keeping specific distances from the centrosome over time (high density of granules exhibiting uniform behavior indicated by yellow in Fig. 4 d). In contrast, with reduced signal strength we found a more heterogeneous distribution of granule-to-centrosome distance (lower density of granules exhibiting any particular behavior indicated by green/blue in Fig. 4, e and f). To track both granules and the centrosome, we classified both as docked when <1 µm from the synapse (Fig. 4, g–l). Using the strongest signal strength (N4), 90% polarized both centrosome and granules together, while with the weakest, G4, 80% did so. Thus, granule delivery via centrosome docking could be achieved by CTLs regardless of stimulation strength. Overall, 93% of CTLs in which centrosome docking was seen also showed concomitant granule delivery of at least one granule to within <0.5 µm of the synapse, demonstrating that this pattern is shared across stimuli (Fig. S3). Hence, the increased frequency of centrosome docking with high-affinity ligands (N4) also increased a coordinated delivery of granules to the synapse.

Ca^{2+} flux precedes uropod retraction and centrosome docking

As Ca^{2+} flux is required for both centrosome polarization (Yi et al., 2013) and granule release (Maul-Pavicic et al., 2011), we asked how calcium flux relates to centrosome polarization. OTI CTLs were transfected with the GCaMP6 Ca^{2+} biosensor (Chen et al., 2013) before imaging with N4-presenting fluorescent-EL4 (Fig. 5, a–c; and Video 4). We found that 42% of CTLs generated a Ca^{2+} flux within 30 s, and all CTLs generated an initial Ca^{2+} flux with a mean time of 55 s (median, 46 s; Fig. 5 d). In those CTLs where a uropod could be identified, we noted that it retracted soon after the first Ca^{2+} flux (mean, 91.7 s; median, 66.5 s), closely followed by the start of centrosome polarization (mean, 94 s; median, 70 s; Fig. 5, e and f). In 50% of CTLs, the centrosome docked within 5 min of the initiation of the first Ca^{2+} flux, with a mean time of 428 s (Fig. 5 g). This matched well with previous observations calculated from the time of first contact. Hence, Ca^{2+} flux precedes uropod retraction and centrosome docking.

We next asked how the strength of signal varied these responses (Fig. 6 a and Video 5). Quantitation of 4D imaging showed that as TCR signal strength increased, the median duration of the primary calcium flux also increased, from 30 s for the null peptide NP68 to 60 s for weak (G4) and 100 s for strong (N4) TCR signaling (Fig. 6 b). Hence, increasing TCR signal strength increased the frequency of a prolonged primary calcium flux.

We examined the relationship between the duration of the first Ca^{2+} flux and centrosome docking by identifying the closest centrosome-to-synapse position within a 40-min window (Fig. 6 c). CTL centrosomes were classed as in the uropod: distal (>5 µm), proximal (1–5 µm), or docked (<1 µm; Fig. 6, c and d). CTLs in which the centrosome was only ever observed in the uropod or >1 µm from the synapse showed initial calcium fluxes with means of ∼60 s. In CTLs where centrosome docking was successful, the mean Ca^{2+} duration was 207 s (median, 190 s) and always >50 s (Fig. 6 c). Although CTLs from each stimulation condition could generate Ca^{2+} fluxes of >50 s, a higher proportion of CTLs stimulated with N4 achieved centrosome docking (Fig. 6 d). These data suggest that increased signal strength increases the duration of Ca^{2+} flux and the frequency of centrosome docking. Thus, increased strength of signal leads to an increased frequency of CTLs with longer dwell times, Ca^{2+} fluxes, and resultant centrosome and granule polarization, all favoring CTL-mediated killing.

Discussion

Increasing TCR signal strength increases the killing efficiency of a target population

Many different studies have found that increasing the strength of TCR–pMHC affinity increases killing of target cells as measured by target cell death or CTL degranulation. However, how the changing strength of TCR signaling controls the cell biology of CTL killing has remained largely unexplored.

Most previous investigations have used end point analyses of conjugation efficacy, including microscopy and flow cytometry of fixed CTL target conjugates (Jenkins et al., 2009; Palmer et al., 2016; Yachi et al., 2006). Although imaging suggested an increased conjugation frequency with higher TCR affinity, the trend was weak and could be explained by an inability to distinguish long-lived TCR-dependent interactions from short-lived target sampling as observed with CTLs cultured with NP68 presenting targets. A much stronger impact of TCR signal strength on conjugation frequency was seen using flow cytometry (Palmer et al., 2016). However, as the authors pointed out, the strength of adhesion may affect the estimation of the frequency of conjugated cells when using flow cytometry, arguing for a role of TCR signal strength in the formation of a stable synapse. Combining flow cytometry with a time course, showed the percentage of conjugated cells rapidly increased over the first 15 min with high-affinity (N4) compared with low-affinity (G4) ligands; however, conjugate frequencies equalized by 30 min (Yachi et al., 2006).

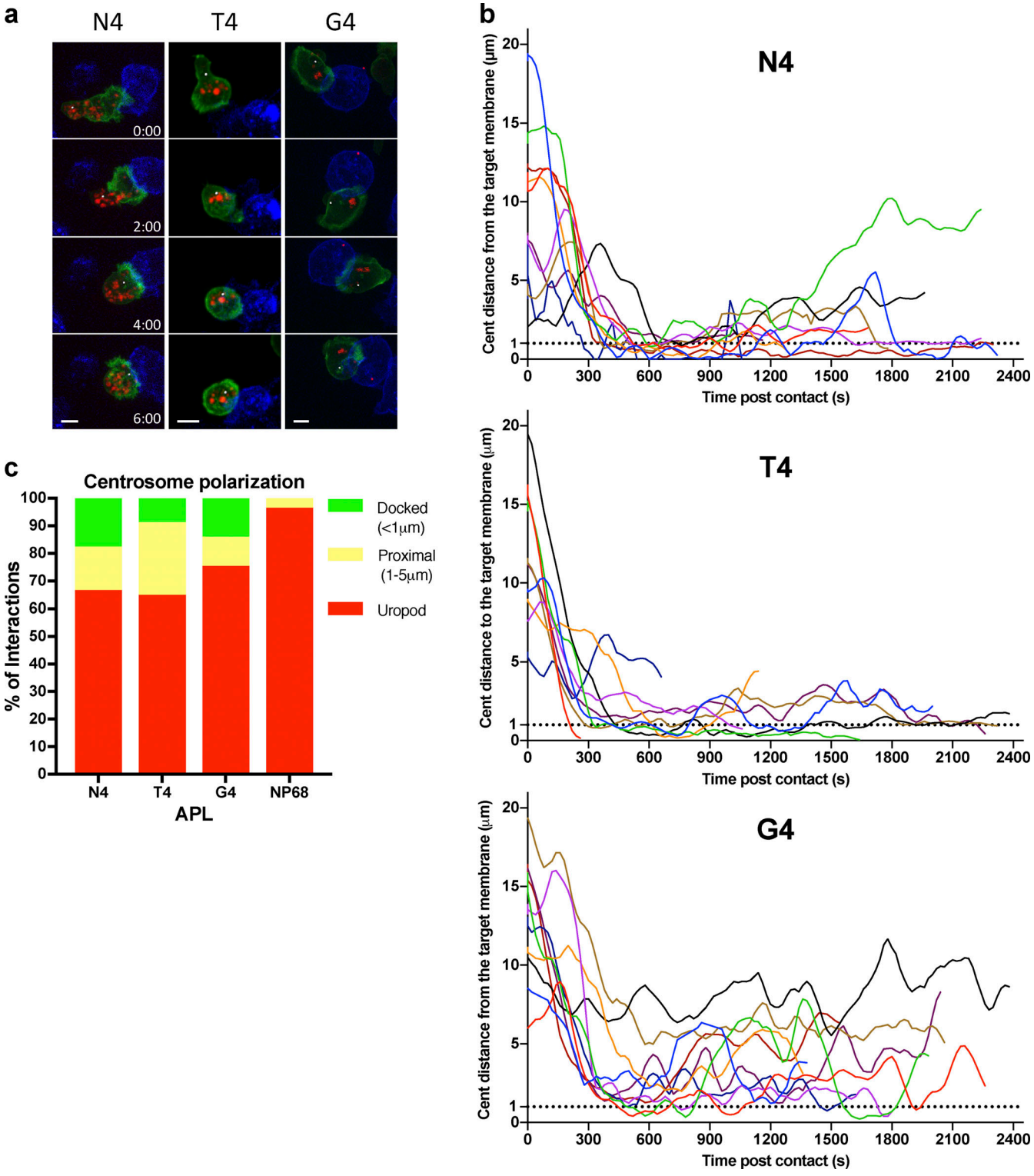

Figure 3. **Increasing TCR signal strength increases centrosome (cent) docking at the synapse.** GzmB-TdTomato (red) OTI CTLs expressing Lifeact-EGFP (green) and BFP-PACT (white sphere) interacting with EL4 (blue), pulsed with N4, T4, G4, or NP68 peptides. **(a)** Representative maximum-intensity projection time series of OTI CTLs encountering targets. Scale bars = 5 μm; time min:s after contact with target. **(b)** Segmented centrosome distances to synapse measured across the duration of the interaction for n = 10 (N4, G4) or n = 9 (T4) independent CTL–target interactions, with each color representing a different CTL. **(c)** OTIs expressing LifeAct-mApple and RFP-PACT were imaged every 10 s over 40 min interacting with EL4-blue, pulsed with N4, T4, G4, or NP68. The closest approach of the centrosome to the target cell membrane per interaction was classified as in the uropod (>5 μm), proximal (1–5 μm), or docked (<1 μm). Results from five independent experiments, with CTL N4 = 58, T4 = 57, G4 = 80, and NP68 = 126, and total interactions analyzed, N4 = 121, T4 = 129, G4 = 169, and NP68 = 284.

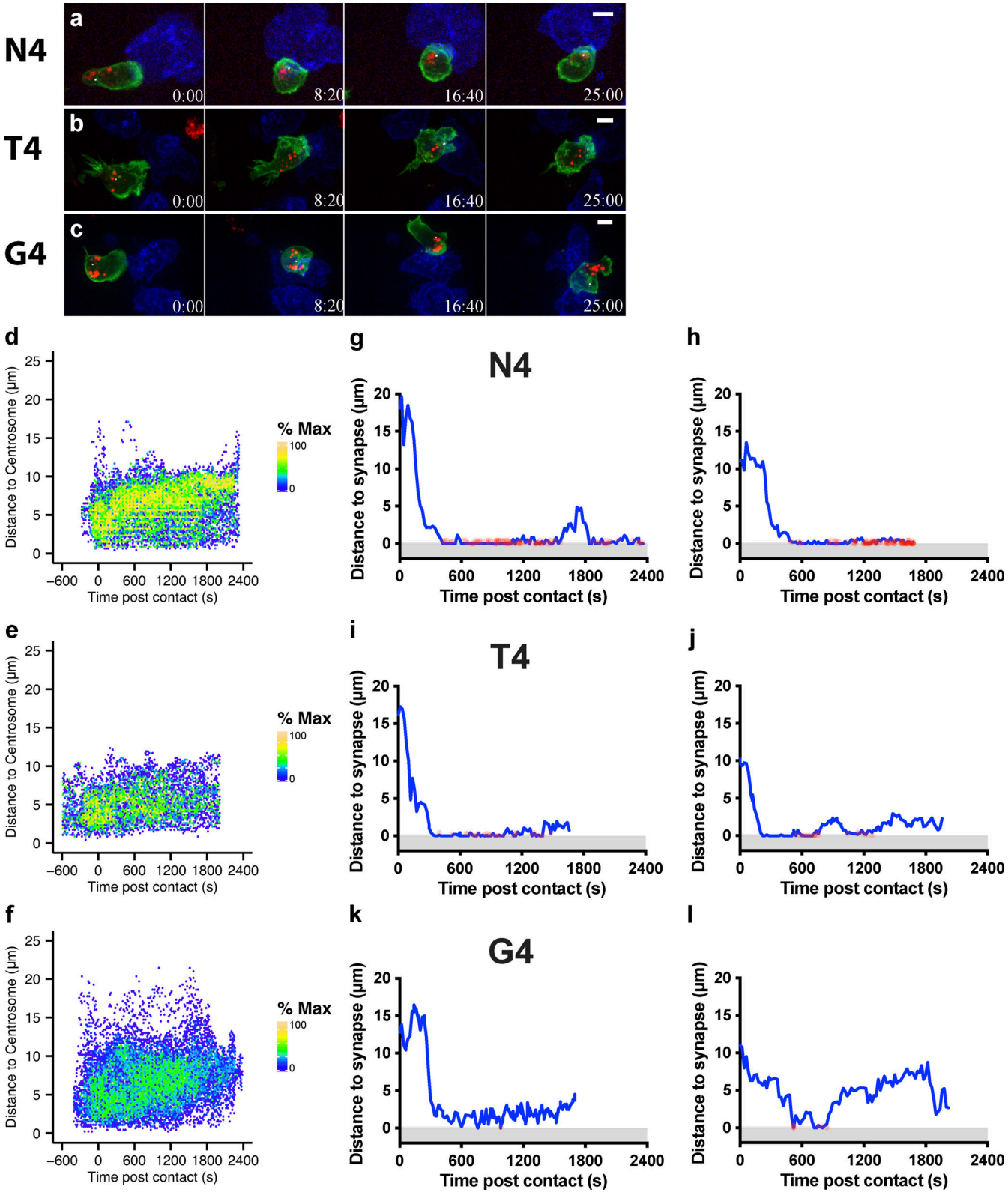

Figure 4. **Prolonged docking of the centrosome to the synapse promotes granule delivery to the synapse.** GzmB-TdTomato (red) OTI CTLs expressing Lifeact-EGFP (green) and BFP-PACT (white sphere) interacting with EL4 (blue), pulsed with N4, T4, or G4 peptides. **(a–c)** Representative maximum-intensity projection time series of OTI CTLs encountering APL pulsed targets. Scale bars = 5 µm; time min:s after contact with target. **(d–f)** Normalized heatmap of granule-to-centrosome distances from segmented CTL target interactions shown in Fig. 3 b. Color scale represents the density of granules relative to the maximum density on each plot. Total granule-to-centrosome distances measured, *n* = 15,192 (d), *n* = 20,343 (e), and *n* = 16,443 (f). **(g–l)** R was used to filter granules for concomitant centrosome docking and granule delivery (<0.5 µm of the synapse) and plot them as red spots on a blue trace showing centrosome distance from the synapse. Two representative cells are shown per APL, from a total of N4 = 10, T4 = 9, and G4 = 10.

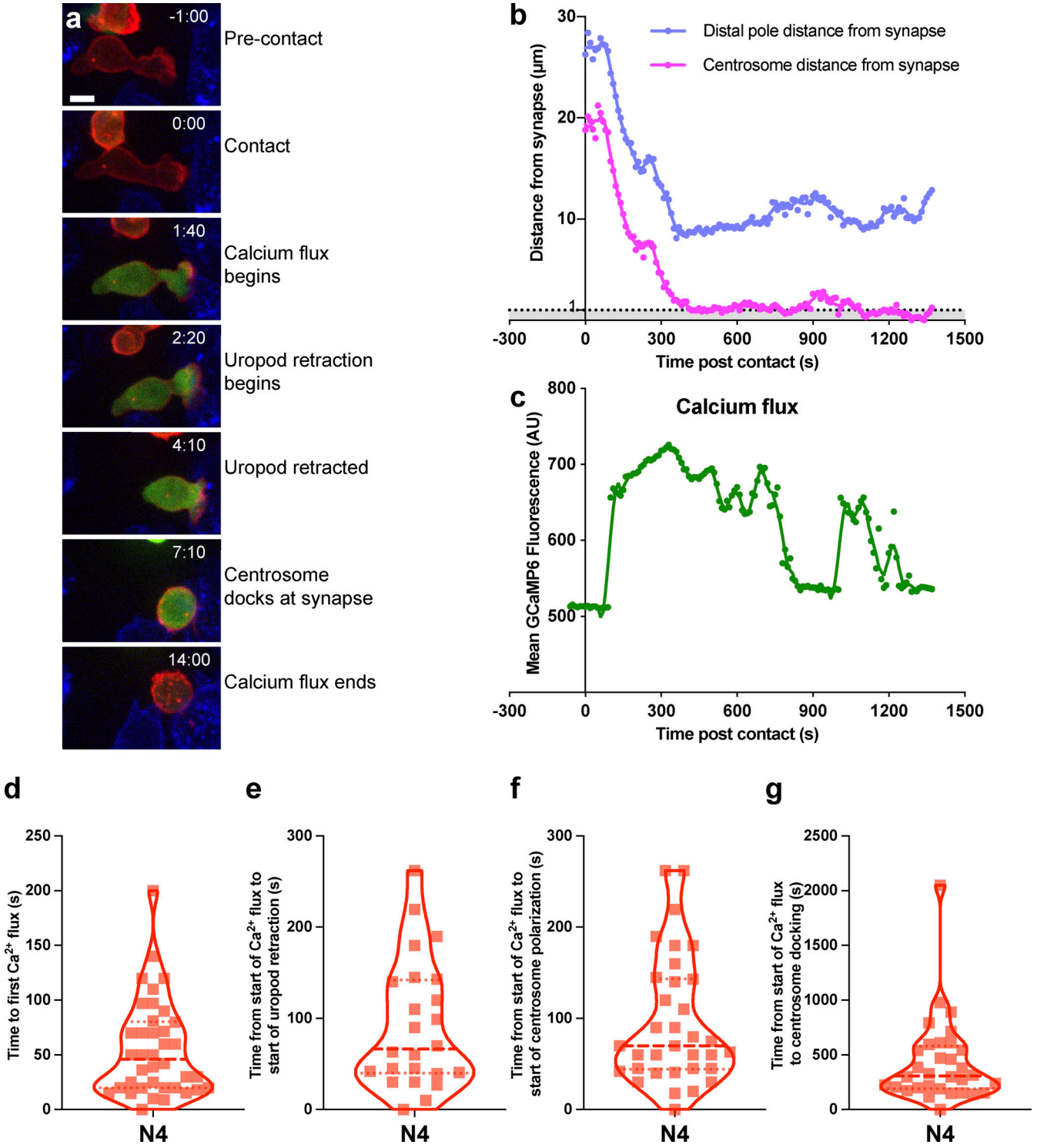

Figure 5. **Calcium flux precedes centrosome polarization and uropod retraction.** OTI CTLs expressing GCAMP6m (green), Lifeact-mApple (red), and RFP-PACT (red sphere) interacting with EL4 (blue), pulsed with N4. **(a)** Representative maximum-intensity projection time series of OTI CTLs encountering N4 pulsed target. Scale bars = 5 µm; time min:s after contact with target. **(b and c)** Example cell from (a) segmented using Imaris to measure the distance of the distal pole (blue) and centrosome (red) to the synapse (b), and the mean GCaMP6m fluorescence within the CTL (c). **(d–g)** Violin plots of time from contact to first calcium flux (d; *n* = 38), the time from the start of the calcium flux to start of uropod retraction (e; *n* = 24), start of centrosome polarization toward synapse (f; *n* = 34), and centrosome docking at the synapse (g; *n* = 32).

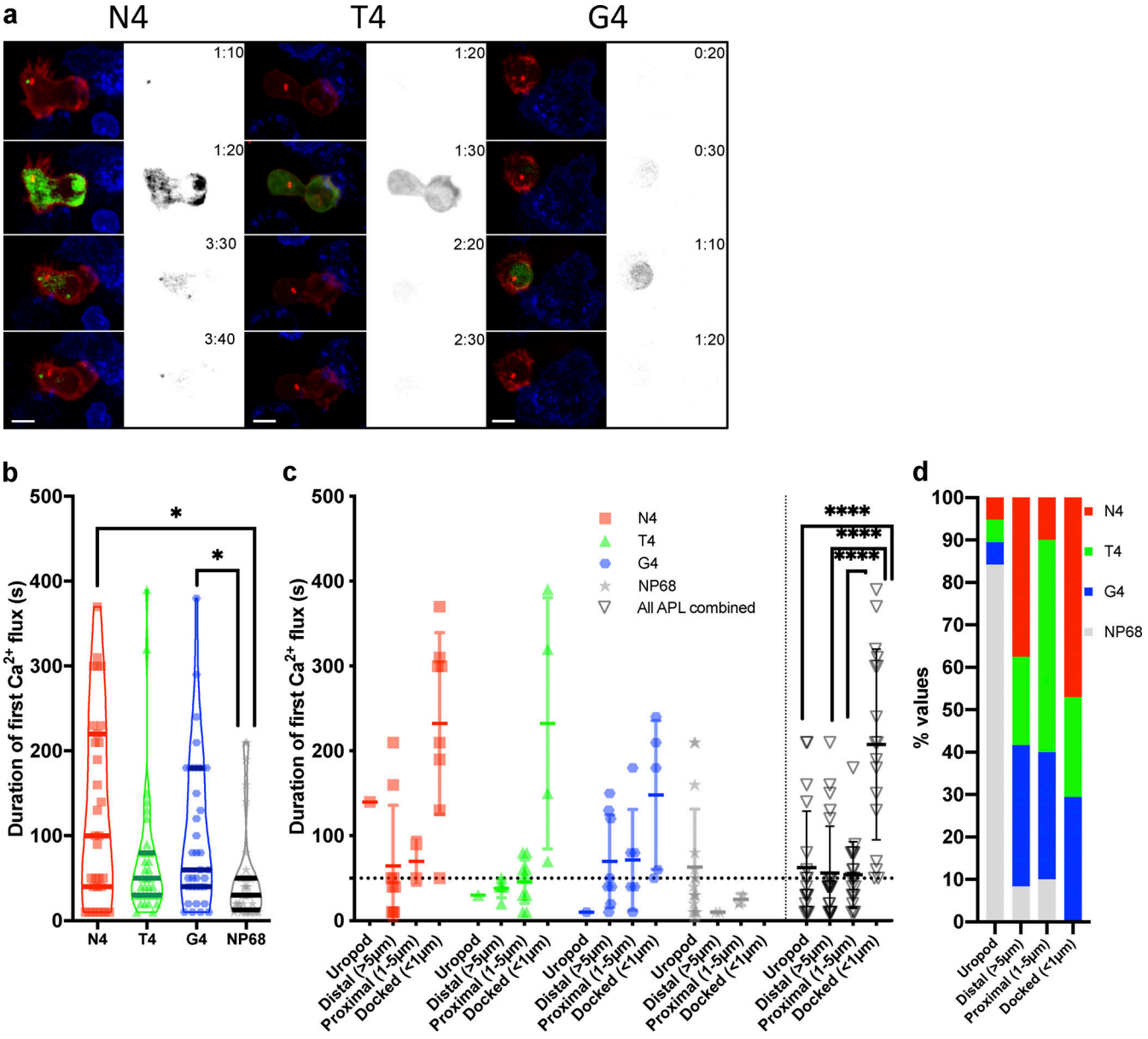

Figure 6. **Duration of initial calcium fluxes are increased with higher-affinity ligands.** OTI CTLs expressing GCAMP6m (green), Lifeact-mApple (red), and RFP-PACT (red sphere) interacting with EL4 (blue), pulsed with N4, T4, or G4. **(a)** Representative maximum-intensity projection time series of OTI CTLs encountering APL pulsed targets. Scale bars = 5 µm; time min:s after contact with target (right, monochrome) fluorescence in the GCaMP6 channel. **(b and c)** The duration of the first increase in GCaMP6 fluorescence within an interaction (b; N4 *n* = 31, T4/G4 *n* = 35, and NP68 *n* = 36). Bars show medians with quartiles duration of the first increase in GCaMP6 fluorescence within an interaction (c; *n* = 20/APL downsampled from [b]). Measurements have been grouped in (c) and (d) by the APL presented by the target (symbol/color) and by the closest approach of the centrosome to the target membrane. Bars show mean ± SD. **(d)** All data from (c) combined to show the percentage of cells for each APL with a given centrosome position. Statistics: Bonferroni-corrected Mann–Whitney test. *, P < 0.05; ****, P < 0.00001.

Using live cell imaging, we now find that lower-strength interactions (that give rise to asynchronous activation) decreased the dwell times of CTLs with targets. Hence, as signal strength increases, the probability of a CTL–target interaction being long-lived increases. Consequently, high-affinity interactions result in rapid and synchronous conjugate formation, while lower-affinity interactions require longer to form the same number of conjugates in a bulk population.

Interestingly, dwell time of naive CD8 T cells has also been shown to increase with higher-affinity TCR ligands (Le Borgne et al., 2016; Moreau et al., 2012; Ozga et al., 2016; Zahm et al., 2017). It is argued that this prolonged dwell time allows naive T cells to maximize the activation signals received from the antigen-presenting cell and mount the stronger peripheral responses seen with stronger TCR signals. Our current study does not address the possibility that multiple weak-affinity interactions can accumulate in CTLs, leading to higher levels of intracellular activation. Likewise, in vivo studies with two-photon microscopy of CTLs killing virally infected cells was also unable to determine whether single CTL killing rates increased

or decreased after sequential target encounters (Halle et al., 2016).

Strong TCR signaling promotes the loss of charge and resulting depletion of actin from the synapse

Many studies have shown dynamic changes in the actin cytoskeleton across the immune synapse (Blumenthal and Burkhardt, 2020). Early studies suggested that weak signals reduced actin polymerization at the synapse (Palmer et al., 2016), although actin depletion could be observed in CTLs with both N4 and G4 generated conjugates (Jenkins et al., 2009). More recent data have revealed a clear molecular link between TCR signaling and actin depletion, whereby TCR ligation triggered changes in the phosphoinositide composition with a loss of PIP2 and decreased membrane charge leading to depletion of actin across the synapse (Gawden-Bone et al., 2018). This predicts that stronger signals should generate greater actin depletion. Testing this hypothesis, we found that both loss of membrane charge and actin depletion were greater with higher-affinity ligands (N4). Consistent with our findings, a recent study in $CD4^+$ T cells also found that stronger TCR signals resulted in decreased levels of PIP2 compared with weaker TCR signals (Hawse and Cattley, 2019).

Increasing TCR signal strength promotes centrosome polarization to the synapse

Centrosome polarization and docking within the synapse is a crucial step in the killing process (Stinchcombe et al., 2006; Stinchcombe et al., 2015). The accumulation of diacylglycerol at the synapse has been shown to trigger centrosome polarization and be required for CTL killing, with centriole deletion (formed after Sas4/p53 deletion) resulting in reduced killing (Quann et al., 2009; Tamzalit et al., 2020). Dynein at the immune synapse is thought to play a role in generating the forces required for centrosome translocation (Combs et al., 2006; Stinchcombe et al., 2006; Yi et al., 2013). The movement of the centrosome has been shown to be biphasic, with dynein-mediated end-on capture shrinkage of "pioneer" microtubules drawing the centrosome into the proximity of the synapse rapidly, before it slowly moves to associate with the membrane (Yi et al., 2013). Other proteins involved in microtubule dynamics have also been implicated, including the kinesin-4 protein KIF21B, which facilitates centrosome polarization by limiting the growth of microtubules (Hooikaas et al., 2020). Although studies using N4 stimulation have described similar rates of centrosome polarization (Ritter et al., 2015; Yi et al., 2013), whether the rate of centrosome polarization changes according to TCR signal strength had not been explored.

In this study we determined the speed with which the centrosome moved toward the synapse by measuring the centrosome-to-synapse distance over time. We found that as TCR signal strength increased, the speed of centrosome movement toward the synapse did not change, although the rate at which a CTL population achieved centrosome docking at the synapse increased. This indicates that the underlying mechanics of centrosome polarization are independent of TCR signal strength. However, the rate at which centrosome polarization was triggered within the CTL population increased with signal strength. We noted that the centrosome polarized and retracted from the synapse multiple times with weaker TCR signals, contributing to a much greater heterogeneity of centrosome docking within the population. Thus, the success of centrosome docking paralleled the success of killing. Our data therefore support a critical role for centrosome docking in killing.

Docking of the centrosome promotes simultaneous delivery of granules to the synapse

Our results suggest that granules cluster around the centrosome for the first 5 min of an interaction (Fig. 4), but then the majority disperse, leaving a small percentage close to the centrosome. As TCR signal strength increased, granules maintained a more uniform distance from the centrosome, as indicated by the yellow intensity (Fig. 4, d–f). Previous studies using imaging of fixed cells suggested that granule clustering is impaired with weak TCR signals (Beal et al., 2009; Jenkins et al., 2009), while live imaging showed mean granule distance from the centrosome gradually increased ∼2–3 min after centrosome docking (Ritter et al., 2015). Our data now resolve these results by showing that increasing TCR signal strength increases the proportion of cells in which coordinated delivery of granules to the synapse is successful.

Ca^{2+} flux precedes uropod retraction and centrosome docking

Early work showed Ca^{2+} flux is important in CTL recognition and killing of target cells (Lancki et al., 1987; Takayama and Sitkovsky, 1987), with Ca^{2+} flux preceding cell rounding (Donnadieu et al., 1994; Negulescu et al., 1996) and delivery of the lethal hit (Poenie et al., 1987; Zhou et al., 2018). However, the timing relative to centrosome polarization and docking had been overlooked. We now find that the initial CTL Ca^{2+} flux in response to strong TCR signal (N4) occurs rapidly upon target contact, before uropod retraction and centrosome docking at the synapse. We also noted that as TCR signal strength increased, so too did the predominance of CTLs displaying a prolonged Ca^{2+} flux rather than many short oscillating fluxes, agreeing with single-cell measurements of Ca^{2+} flux distinguishing these populations (Chen et al., 2010; Christo et al., 2015; Dong et al., 2017; Frick et al., 2017; Le Borgne et al., 2016; Liu et al., 2014; Wülfing et al., 1997; Xia et al., 2018).

The role of Ca^{2+} in centrosome polarization has been controversial (Ritter et al., 2013), and previous studies have been limited to using Ca^{2+} chelation or fluorophores best suited to bulk populations. The availability of GCaMP6 and live imaging provided a new opportunity to investigate the links between Ca^{2+} fluxes and centrosome polarization. We found multiple Ca^{2+} fluxes during a single interaction, noting a Ca^{2+} flux of at least 50 s was necessary, if not sufficient, for centrosome docking regardless of signal strength. Furthermore, we found that increasing TCR signal strength increased the proportion of interactions leading to a Ca^{2+} flux >50 s. It is possible that phosphorylation of LAT Y132, which plays a role in ligand discrimination by driving more rapid Ca^{2+} fluxes, contributes to this fine tuning (Lo et al., 2019). Thus, our findings suggest that stronger signals reduce the heterogeneity of the Ca^{2+} fluxes within the population, favoring centrosome docking.

A rate-based mechanism for T cell activation controls polarization

Recent single-cell studies on the activation of naive CD8⁺ T cells have revealed that the changes within populations are controlled by the rate at which conserved TCR signaling pathways activate within individual cells (Ma et al., 2020). Likewise, the transcriptional trajectory following TCR activation is conserved regardless of the strength of TCR signal, but the rate at which individual cells initiate activation increases with increasing strength of signal (Richard et al., 2018). Consequently, within a population, increasing signal strength will increase the number of cells that have activated. These results suggest that both at the signaling and transcriptional levels, naive T cell activation pathways are conserved, but the rate at which individual cells initiate their progress along these pathways changes with strength of signal. Our results examining activated CD8+ T cells (i.e., CTLs) now show that TCR signal strength controls efficient CTL killing of a target population through modulating heterogeneity within the population at multiple distinct stages. These include dwell time, initial Ca^{2+} flux duration, membrane specialization, centrosome docking, and granule clustering and delivery to the synapse. The proportion of CTLs engaged in each step of this process was greater with increased TCR signal strength. Consequently, strong signals gave rapid and homogeneous responses, while weak signals generated much more heterogeneity, reducing the rate of target killing. We found that those cells that reached full activation showed centrosome docking and granule polarization regardless of the initial signal strength. Furthermore, pathways leading to successful granule delivery, such as the speed of centrosome movement, were conserved across all signal strengths. Our results are consistent with an emerging model of signal strength controlling the rate of progression along conserved pathways, as seen for transcriptional activation and intracellular signaling in naive T cells (Ma et al., 2020; Richard et al., 2018). This model explains the delayed kinetics of weak ligand responses in bulk populations that were often interpreted as slowed rather than asynchronous responses.

Materials and methods

DNA constructs

BFP-PACT in the pTagBFP-C (Evrogen) vector, RFP-PACT (Gillingham and Munro, 2000), mApple-LifeAct-7 (Addgene plasmid #54747), and EGFP-LifeAct-7 (Addgene plasmid #54610; Riedl et al., 2008) were as used in Ritter et al. (2015). LAMP-1-mApple and EGFP-Kras8⁺ (Yeung et al., 2008) were gifts from M. Davidson (University of Florida, Gainesville, FL) and Sergio Grinstein (University of Toronto, Toronto, Canada), respectively. GCaMP6m was a gift from Douglas Kim (Janelia Farm Research Campus, Ashburn, VA; Addgene plasmid #40754; Chen et al., 2013).

Mice

C57BL/6 (B6)-OTI Rag2$^{-/-}$ (B6.129S6-Rag2tm1Fwa Tg[TcraTcrb] 1100Mjb), mice referred to as OTI mice, and GzmB-TdTomato OTI mice, referred to as GzmB-TdTom OTI, gifted from Claude Boyer (Mouchacca et al., 2013), were bred and maintained in specific pathogen–free conditions. Experiments were performed under Project Licence PPL 70/8590. This research has been regulated under the Animals (Scientific Procedures) Act 1986 Amendment Regulations 2012 following ethical review by the University of Cambridge Animal Welfare and Ethical Review Body.

Cell culture

Naive OTI splenocytes were stimulated with 10 nM SIINFEKL (Cambridge Bioscience) for 3 d in RPMI 1640 medium (Sigma-Aldrich; Cat# 1640) with 10% FBS (LabTech; Cat# FBS-SA), 50 µM β-mercaptoethanol (Thermo Fisher Scientific; Cat# 31350010), 10 U/ml recombinant murine IL-2 (Peprotech; Cat# 212–12), 2 mM L-glutamine (Sigma-Aldrich; Cat# G7513-100ML), 1 mM sodium pyruvate (Thermo Fisher Scientific; Cat# 11360070), and 50 U/ml penicillin and streptomycin (Sigma-Aldrich; Cat# P0781-100ML). Cells were washed and seeded into fresh media on a daily basis from 3 d after stimulation. Target EL4 and fluorescent EL4 cells (Ritter et al., 2015) were maintained in DMEM (Sigma-Aldrich; Cat# D5030-10X1L) supplemented with 10% FBS and 2 mM L-glutamine.

Peptides and recombinant proteins

$OVA_{257-261}$ SIINFEKL along with all APLs (Q4, SIIQFEKL, Q4R7, SIIKFERL; T4, SIITFEKL, Q4H7, SIIQFEHL; G4, SIIGFEKL) and the NP68 ASNENMDAM were obtained from Cambridge Bioscience. Recombinant mouse ICAM-1/CD45 Fc Chimera Protein Recombinant ICAM1 was obtained from R&D systems (Cat# 796-IC).

Killing assay

Cytotoxic function was assessed with the Promega Cytotox 96 Non-radioactive cytotoxicity assay (Promega; Cat# G1780). EL4 cells were pulsed for 1 h with 1 µM APLs at 37°C 8% CO_2 and washed three times in phenol-red-free RPMI and 2% BSA (Sigma-Aldrich; Cat# A7906-500G; killing assay medium), and 10^4 pulsed EL4 cells were resuspended with CTLs at effector-to-target ratios shown in Fig. S1 a. After 2 h 37°C 8% CO_2, supernatant was collected, and LDH activity at RT was detected by absorbance reading after 30-min exposure at 490 nm with a VERSAmax spectrophotometer (Molecular Devices). Percent lysis was calculated as follows: [(effector induced cell death – blank) – (effector spontaneous death – blank) – (target spontaneous death)]/[(Lysed targets – lysis control) – (target spontaneous death – blank)].

Degranulation assay

EL4 cells were pulsed for 1 h with 1 µM APL at 37°C 10% CO_2 before washing in RPMI and 10% FBS. CTLs and EL4 were mixed 1:1 and plated in triplicate at 2 × 10^5/ml in 200 µl per well with 4 µg/ml PE–anti-LAMP-1 (BioLegend; clone 1D4B). At the stated time points, cells were washed with ice-cold PBS before fixing with 2% PFA (Electron Microscopy Sciences; Cat# 15710-S) and PBS for 10 min at RT. Cells were then washed in PBS and 1% FBS (FACS buffer) and left at 4°C until all time points had been collected. Cells were stained with APC–anti-mouse CD8α (BioLegend; clone 53–6.7) for 30 min at 4°C before data acquisition

with a BD FACSCalibur. CTLs were gated on FSCvSSC for lymphocytes, then CD8$^+$ cells before analyzing the percentage of LAMP-1$^+$ and geometric mean PE fluorescence.

Immunofluorescence imaging of actin in fixed cells

24 h before the experiment and 5–8 d after stimulation, 5 × 10^6 OTI CTLs were transfected with 5 µg of DNA containing the EGFP-Kras8$^+$ probe using the Mouse CD8 T cell nucleofection kit (Amaxa). EL4-expressing Farnesyl-5-TagBFP2 were pulsed with 1 µM APL for 1 h at 37°C, washed three times, and resuspended at 10^6 cells/ml together with 10^6 cells/ml OTI cells expressing EGFP-Kras8$^+$ (1:1 ratio). CTLs and targets were allowed to form conjugates at 37°C for 5 min before being placed on 5-well slides (Hendley; Cat# P299) using a cut-off pipette tip and incubated at 37°C, 10% CO_2 for the times shown in Fig. 2. Conjugates were fixed in 4% PFA at RT for 5 min, washed in PBS, quenched in PBS and 50 mM ammonium chloride (Sigma-Aldrich; Cat# 254134) for 10 min, permeabilized with 0.2% Triton X-100 (Sigma-Aldrich;Cat# T8787-100ML) and PBS for 5 min RT, and blocked with PBS and 1% BSA for 1 h at 4°C before labeling with mouse anti-phosphotyrosine 4G10 (Merck/Millipore; Cat# 05–1050) and donkey anti-mouse (H+L) 647 Alexa Fluor secondary antibody (Thermo Fisher Scientific; Cat# A32787) with Phalloidin-Alexa-555 (Invitrogen; Cat# A34055). Samples were mounted in ProLong Diamond Antifade Mountant (Thermo Fisher Scientific; Cat# P36961) with a no. 1.5 coverslip and imaged at RT using an Andor system, with an Olympus IX81S1F-3-5 body, Piezo Z, and motor XY stage control (H117E2IX), Yokogawa CSU-X1 spinning disk, and iXon Ultra 888 camera (Andor) with Andor IQ3 software (Olympus Plan Appochromat 100× 1.4 NA oil objective and z-step distance of 0.2 µm). Images were analyzed using Bitplane Imaris 8.3.1 and en face images generated using an oblique slice of 3 µm thick, which was exported to ImageJ for further quantification. Intensity profiles were acquired using the line tool analysis, and percent synapse area depleted was calculated as 100 × [1 – ([area of synapse above background threshold]/[area of synapse above threshold with gaps filled in])].

Live microscopy

24 h before imaging and 5–8 d after stimulation, 5 × 10^6 CTLs were transfected with 5–16 µg DNA using the Mouse CD8 T cell nucleofection kit (Amaxa; Cat# VPA-1006). EL4s expressing either Farnesyl-5-TagBFP2 or Mem-RFP670 were used as targets and pulsed for 30 min with 1 µM peptide at 37°C and 8% CO_2 before washing into serum-free DMEM and applying to 1 µg/ml murine ICAM-1–coated 35-mm glass-bottomed culture dishes at 6.5 × 10^5/ml. After 5 min to adhere, unbound targets were washed clear with phenol-red free T cell medium plus 25 mM Hepes, and the dish was loaded onto the microscope. Approximately 2 × 10^6 nucleofected CTLs were dropped onto the dish, and imaging began within 5 min.

Imaging of CTL:Target interactions used the system described above with an Olympus Universal Plan Super Apochromat 60× 1.3 NA silicone oil objective and an OKOLAB stage incubator to maintain a 37°C temperature and ∼5% CO_2 atmosphere. Each z-plane was separated by 0.8 µm with the z-dimension ranging from 16–20 µm and image stacks taken every 5–20 s for 20–40 min. Fluorophores were excited with 405-, 488-, 561-, and 640-nm lasers in each plane. Data were captured with the iQ3 software (Andor) before visualizing and analyzing with Imaris (Bitplane).

Live cell object-based image analysis

To measure Ca^{2+} flux and follow centrosome-to-granule and/or -synapse distances over time, these structures were segmented with the Bitplane Imaris software. In brief, the boundaries of the CTL and target were segmented using the Imaris surface function on the LifeAct signal for the CTL and the relevant signal for the target membrane as the target cell. Cytotoxic granules were identified using the spots function on the RFP-fluorescent signal, and the centrosome was detected with the spots function on the PACT signal. The Imaris cell function was then used on these boundaries to measure the intracellular distance from the immune synapse to the centrosome or the centrosome to the cytotoxic granules. Where just the centrosome distance to the synapse was measured, the synapse was represented as a surface where the target and CTL objects overlapped, and the shortest distance was calculated. In contrast, where centrosome-to-granule distances were concurrently measured, it was required to convert the synapse surface to spots and manually limit these to provide an equivalent shortest distance, but with repeat measurements to account for the introduced human error. Rstudio 1.0.136 (Rstudio, Inc.) with R version 3.0.2 (R Foundation for Statistical Computing) and ggplot2 (Wickham, 2009) was used to plot granule-to-centrosome distances as a hexbin density plot, as well as filter centrosome– and granule–to–immune synapse distance as <0.5 µm for Fig. 4 and Fig. S3. Calcium fluorescence was calculated as the mean GFP intensity within the bounds of the CTL surface. For greater detail, see Frazer et al. (2017).

Live cell manual analysis

The primary calcium flux length was measured from the first frame the GCaMP6m fluorescence visibly exceeded background until the frame where it returned to this intensity. Centrosome-to-synapse distances were measured within the central plane of the PACT fluorescence from the center of this structure to the target fluorescence using the Imaris distance tool. Interactions were assumed when the CTL LifeAct signal appeared to touch the target membrane, and dwell time was measured until this ceased. This signal was also used to determine the presence and retraction of the uropod.

Statistics

A two-tailed Bonferroni-corrected Mann–Whitney test was used for all statistical analyses.

Online supplemental material

Fig. S1 shows that stronger TCR signal strengths increase CTL killing efficiency. Fig. S2 shows that centrosome speed is unaffected by TCR signal strength. Fig. S3 examines centrosome and granule docking. Video 1 shows that increasing TCR signal strength increases CTL dwell time. Video 2 shows that increasing TCR signal strength increases centrosome docking at the synapse.

Video 3 demonstrates that prolonged docking of the centrosome to the synapse promotes granule delivery to the synapse. Video 4 shows that calcium flux precedes centrosome polarization and uropod retraction. Video 5 reveals that the duration of initial calcium fluxes is increased with higher-affinity ligands.

Acknowledgments

We would like to thank Arianne Richard and Alice Denton for helpful discussions and critical review of the manuscript, and the Cambridge Institute for Medical Research flow cytometry core facility.

This work was funded by grants from the Wellcome Trust (103930, 099789, 097024, 100140, and 217100). This research was funded in whole or in part by Wellcome Trust. For the purpose of Open Access, the author has applied a CC-BY public copyright license to any Author Accepted Manuscript (AAM) version arising from this submission.

The authors declare no competing financial interests.

Author contributions: G.L. Frazer, N.M.G. Dieckmann, C.M. Gawden-Bone, and Y. Asano conducted experiments; G.L. Frazer and G.M. Griffiths wrote the manuscript; and all authors edited and approved the manuscript.

Submitted: 20 April 2021
Revised: 3 June 2021
Accepted: 30 June 2021

References

Alam, S.M., P.J. Travers, J.L. Wung, W. Nasholds, S. Redpath, S.C. Jameson, and N.R.J. Gascoigne. 1996. T-cell-receptor affinity and thymocyte positive selection. *Nature.* 381:616–620. https://doi.org/10.1038/381616a0

Alam, S.M., G.M. Davies, C.M. Lin, T. Zal, W. Nasholds, S.C. Jameson, K.A. Hogquist, N.R. Gascoigne, and P.J. Travers. 1999. Qualitative and quantitative differences in T cell receptor binding of agonist and antagonist ligands. *Immunity.* 10:227–237. https://doi.org/10.1016/S1074-7613(00)80023-0

Beal, A.M., N. Anikeeva, R. Varma, T.O. Cameron, G. Vasiliver-Shamis, P.J. Norris, M.L. Dustin, and Y. Sykulev. 2009. Kinetics of early T cell receptor signaling regulate the pathway of lytic granule delivery to the secretory domain. *Immunity.* 31:632–642. https://doi.org/10.1016/j.immuni.2009.09.004

Blumenthal, D., and J.K. Burkhardt. 2020. Multiple actin networks coordinate mechanotransduction at the immunological synapse. *J. Cell Biol.* 219: e201911058. https://doi.org/10.1083/jcb.201911058

Chen, J.L., A.J. Morgan, G. Stewart-Jones, D. Shepherd, G. Bossi, L. Wooldridge, S.L. Hutchinson, A.K. Sewell, G.M. Griffiths, P.A. van der Merwe, et al. 2010. Ca2+ release from the endoplasmic reticulum of NY-ESO-1-specific T cells is modulated by the affinity of TCR and by the use of the CD8 coreceptor. *J. Immunol.* 184:1829–1839. https://doi.org/10.4049/jimmunol.0902103

Chen, T.W., T.J. Wardill, Y. Sun, S.R. Pulver, S.L. Renninger, A. Baohan, E.R. Schreiter, R.A. Kerr, M.B. Orger, V. Jayaraman, et al. 2013. Ultrasensitive fluorescent proteins for imaging neuronal activity. *Nature.* 499: 295–300. https://doi.org/10.1038/nature12354

Christo, S.N., K.R. Diener, R.E. Nordon, M.P. Brown, H.J. Griesser, K. Vasilev, F.C. Christo, and J.D. Hayball. 2015. Scrutinizing calcium flux oscillations in T lymphocytes to deduce the strength of stimulus. *Sci. Rep.* 5: 7760. https://doi.org/10.1038/srep07760

Combs, J., S.J. Kim, S. Tan, L.A. Ligon, E.L. Holzbaur, J. Kuhn, and M. Poenie. 2006. Recruitment of dynein to the Jurkat immunological synapse. *Proc. Natl. Acad. Sci. USA.* 103:14883–14888. https://doi.org/10.1073/pnas.0600914103

Daniels, M.A., E. Teixeiro, J. Gill, B. Hausmann, D. Roubaty, K. Holmberg, G. Werlen, G.A. Holländer, N.R. Gascoigne, and E. Palmer. 2006. Thymic selection threshold defined by compartmentalization of Ras/MAPK signalling. *Nature.* 444:724–729. https://doi.org/10.1038/nature05269

Denton, A.E., R. Wesselingh, S. Gras, C. Guillonneau, M.R. Olson, J.D. Mintern, W. Zeng, D.C. Jackson, J. Rossjohn, P.D. Hodgkin, et al. 2011. Affinity thresholds for naive CD8+ CTL activation by peptides and engineered influenza A viruses. *J. Immunol.* 187:5733–5744. https://doi.org/10.4049/jimmunol.1003937

Dong, T.X., S. Othy, A. Jairaman, J. Skupsky, A. Zavala, I. Parker, J.L. Dynes, and M.D. Cahalan. 2017. T-cell calcium dynamics visualized in a ratiometric tdTomato-GCaMP6f transgenic reporter mouse. *eLife.* 6:e32417. https://doi.org/10.7554/eLife.32417

Donnadieu, E., G. Bismuth, and A. Trautmann. 1994. Antigen recognition by helper T cells elicits a sequence of distinct changes of their shape and intracellular calcium. *Curr. Biol.* 4:584–595. https://doi.org/10.1016/S0960-9822(00)00130-5

Frazer, G.L., Y. Asano, and G.M. Griffiths. 2017. Imaging the Effector CD8 Synapse. *Methods Mol. Biol.* 1584:473–486. https://doi.org/10.1007/978-1-4939-6881-7_29

Frick, M., P. Mouchacca, G. Verdeil, Y. Hamon, C. Billaudeau, M. Buferne, M. Fallet, N. Auphan-Anezin, A.M. Schmitt-Verhulst, and C. Boyer. 2017. Distinct patterns of cytolytic T-cell activation by different tumour cells revealed by Ca^{2+} signalling and granule mobilization. *Immunology.* 150: 199–212. https://doi.org/10.1111/imm.12679

Gawden-Bone, C.M., G.L. Frazer, A.C. Richard, C.Y. Ma, K. Strege, and G.M. Griffiths. 2018. PIP5 Kinases Regulate Membrane Phosphoinositide and Actin Composition for Targeted Granule Secretion by Cytotoxic Lymphocytes. *Immunity.* 49:427–437.e4. https://doi.org/10.1016/j.immuni.2018.08.017

Gillingham, A.K., and S. Munro. 2000. The PACT domain, a conserved centrosomal targeting motif in the coiled-coil proteins AKAP450 and pericentrin. *EMBO Rep.* 1:524–529. https://doi.org/10.1093/embo-reports/kvd105

Halle, S., K.A. Keyser, F.R. Stahl, A. Busche, A. Marquardt, X. Zheng, M. Galla, V. Heissmeyer, K. Heller, J. Boelter, et al. 2016. In Vivo Killing Capacity of Cytotoxic T Cells Is Limited and Involves Dynamic Interactions and T Cell Cooperativity. *Immunity.* 44:233–245. https://doi.org/10.1016/j.immuni.2016.01.010

Hawse, W.F., and R.T. Cattley. 2019. T cells transduce T-cell receptor signal strength by generating different phosphatidylinositols. *J. Biol. Chem.* 294:4793–4805. https://doi.org/10.1074/jbc.RA118.006524

Hogquist, K.A., S.C. Jameson, W.R. Heath, J.L. Howard, M.J. Bevan, and F.R. Carbone. 1994. T cell receptor antagonist peptides induce positive selection. *Cell.* 76:17–27. https://doi.org/10.1016/0092-8674(94)90169-4

Hogquist, K.A., S.C. Jameson, and M.J. Bevan. 1995. Strong agonist ligands for the T cell receptor do not mediate positive selection of functional CD8+ T cells. *Immunity.* 3:79–86. https://doi.org/10.1016/1074-7613(95)90160-4

Hooikaas, P.J., H.G. Damstra, O.J. Gros, W.E. van Riel, M. Martin, Y.T. Smits, J. van Loosdregt, L.C. Kapitein, F. Berger, and A. Akhmanova. 2020. Kinesin-4 KIF21B limits microtubule growth to allow rapid centrosome polarization in T cells. *eLife.* 9:e62876. https://doi.org/10.7554/eLife.62876

Huang, J., V.I. Zarnitsyna, B. Liu, L.J. Edwards, N. Jiang, B.D. Evavold, and C. Zhu. 2010. The kinetics of two-dimensional TCR and pMHC interactions determine T-cell responsiveness. *Nature.* 464:932–936. https://doi.org/10.1038/nature08944

Jenkins, M.R., A. Tsun, J.C. Stinchcombe, and G.M. Griffiths. 2009. The strength of T cell receptor signal controls the polarization of cytotoxic machinery to the immunological synapse. *Immunity.* 31:621–631. https://doi.org/10.1016/j.immuni.2009.08.024

Kelly, J.M., S.J. Sterry, S. Cose, S.J. Turner, J. Fecondo, S. Rodda, P.J. Fink, and F.R. Carbone. 1993. Identification of conserved T cell receptor CDR3 residues contacting known exposed peptide side chains from a major histocompatibility complex class I-bound determinant. *Eur. J. Immunol.* 23:3318–3326. https://doi.org/10.1002/eji.1830231239

King, C.G., S. Koehli, B. Hausmann, M. Schmaler, D. Zehn, and E. Palmer. 2012. T cell affinity regulates asymmetric division, effector cell differentiation, and tissue pathology. *Immunity.* 37:709–720. https://doi.org/10.1016/j.immuni.2012.06.021

Koniaras, C., F.R. Carbone, W.R. Heath, and A.M. Lew. 1999. Inhibition of naïve class I-restricted T cells by altered peptide ligands. *Immunol. Cell Biol.* 77:318–323. https://doi.org/10.1046/j.1440-1711.1999.00828.x

Lancki, D.W., A. Weiss, and F.W. Fitch. 1987. Requirements for triggering of lysis by cytolytic T lymphocyte clones. *J. Immunol.* 138:3646–3653.
Le Borgne, M., S. Raju, B.H. Zinselmeyer, V.T. Le, J. Li, Y. Wang, M.J. Miller, and A.S. Shaw. 2016. Real-Time Analysis of Calcium Signals during the Early Phase of T Cell Activation Using a Genetically Encoded Calcium Biosensor. *J. Immunol.* 196:1471–1479. https://doi.org/10.4049/jimmunol.1502414
Liu, B., W. Chen, B.D. Evavold, and C. Zhu. 2014. Accumulation of dynamic catch bonds between TCR and agonist peptide-MHC triggers T cell signaling. *Cell.* 157:357–368. https://doi.org/10.1016/j.cell.2014.02.053
Lo, W.L., N.H. Shah, S.A. Rubin, W. Zhang, V. Horkova, I.R. Fallahee, O. Stepanek, L.I. Zon, J. Kuriyan, and A. Weiss. 2019. Slow phosphorylation of a tyrosine residue in LAT optimizes T cell ligand discrimination. *Nat. Immunol.* 20:1481–1493. https://doi.org/10.1038/s41590-019-0502-2
Ma, C.Y., J.C. Marioni, G.M. Griffiths, and A.C. Richard. 2020. Stimulation strength controls the rate of initiation but not the molecular organisation of TCR-induced signalling. *eLife.* 9:e53948. https://doi.org/10.7554/eLife.53948
Maul-Pavicic, A., S.C. Chiang, A. Rensing-Ehl, B. Jessen, C. Fauriat, S.M. Wood, S. Sjöqvist, M. Hufnagel, I. Schulze, T. Bass, et al. 2011. ORAI1-mediated calcium influx is required for human cytotoxic lymphocyte degranulation and target cell lysis. *Proc. Natl. Acad. Sci. USA.* 108:3324–3329. https://doi.org/10.1073/pnas.1013285108
Moreau, H.D., F. Lemaître, E. Terriac, G. Azar, M. Piel, A.M. Lennon-Dumenil, and P. Bousso. 2012. Dynamic in situ cytometry uncovers T cell receptor signaling during immunological synapses and kinapses in vivo. *Immunity.* 37:351–363. https://doi.org/10.1016/j.immuni.2012.05.014
Mouchacca, P., A.M. Schmitt-Verhulst, and C. Boyer. 2013. Visualization of cytolytic T cell differentiation and granule exocytosis with T cells from mice expressing active fluorescent granzyme B. *PLoS One.* 8:e67239. https://doi.org/10.1371/journal.pone.0067239
Naeher, D., M.A. Daniels, B. Hausmann, P. Guillaume, I. Luescher, and E. Palmer. 2007. A constant affinity threshold for T cell tolerance. *J. Exp. Med.* 204:2553–2559. https://doi.org/10.1084/jem.20070254
Negulescu, P.A., T.B. Krasieva, A. Khan, H.H. Kerschbaum, and M.D. Cahalan. 1996. Polarity of T cell shape, motility, and sensitivity to antigen. *Immunity.* 4:421–430. https://doi.org/10.1016/S1074-7613(00)80409-4
Ozga, A.J., F. Moalli, J. Abe, J. Swoger, J. Sharpe, D. Zehn, M. Kreutzfeldt, D. Merkler, J. Ripoll, and J.V. Stein. 2016. pMHC affinity controls duration of CD8+ T cell-DC interactions and imprints timing of effector differentiation versus expansion. *J. Exp. Med.* 213:2811–2829. https://doi.org/10.1084/jem.20160206
Palmer, E., A. Drobek, and O. Stepanek. 2016. Opposing effects of actin signaling and LFA-1 on establishing the affinity threshold for inducing effector T-cell responses in mice. *Eur. J. Immunol.* 46:1887–1901. https://doi.org/10.1002/eji.201545909
Poenie, M., R.Y. Tsien, and A.M. Schmitt-Verhulst. 1987. Sequential activation and lethal hit measured by [Ca2+]i in individual cytolytic T cells and targets. *EMBO J.* 6:2223–2232. https://doi.org/10.1002/j.1460-2075.1987.tb02494.x
Quann, E.J., E. Merino, T. Furuta, and M. Huse. 2009. Localized diacylglycerol drives the polarization of the microtubule-organizing center in T cells. *Nat. Immunol.* 10:627–635. https://doi.org/10.1038/ni.1734
Richard, A.C., A.T.L. Lun, W.W.Y. Lau, B. Göttgens, J.C. Marioni, and G.M. Griffiths. 2018. T cell cytolytic capacity is independent of initial stimulation strength. *Nat. Immunol.* 19:849–858. https://doi.org/10.1038/s41590-018-0160-9
Riedl, J., A.H. Crevenna, K. Kessenbrock, J.H. Yu, D. Neukirchen, M. Bista, F. Bradke, D. Jenne, T.A. Holak, Z. Werb, et al. 2008. Lifeact: a versatile marker to visualize F-actin. *Nat. Methods.* 5:605–607. https://doi.org/10.1038/nmeth.1220
Ritter, A.T., K.L. Angus, and G.M. Griffiths. 2013. The role of the cytoskeleton at the immunological synapse. *Immunol. Rev.* 256:107–117. https://doi.org/10.1111/imr.12117
Ritter, A.T., Y. Asano, J.C. Stinchcombe, N.M. Dieckmann, B.C. Chen, C. Gawden-Bone, S. van Engelenburg, W. Legant, L. Gao, M.W. Davidson, et al. 2015. Actin depletion initiates events leading to granule secretion at the immunological synapse. *Immunity.* 42:864–876. https://doi.org/10.1016/j.immuni.2015.04.013
Ritter, A.T., S.M. Kapnick, S. Murugesan, P.L. Schwartzberg, G.M. Griffiths, and J. Lippincott-Schwartz. 2017. Cortical actin recovery at the immunological synapse leads to termination of lytic granule secretion in cytotoxic T lymphocytes. *Proc. Natl. Acad. Sci. USA.* 114:E6585–E6594. https://doi.org/10.1073/pnas.1710751114
Stinchcombe, J.C., E. Majorovits, G. Bossi, S. Fuller, and G.M. Griffiths. 2006. Centrosome polarization delivers secretory granules to the immunological synapse. *Nature.* 443:462–465. https://doi.org/05071
Stinchcombe, J.C., L.O. Randzavola, K.L. Angus, J.M. Mantell, P. Verkade, and G.M. Griffiths. 2015. Mother Centriole Distal Appendages Mediate Centrosome Docking at the Immunological Synapse and Reveal Mechanistic Parallels with Ciliogenesis. *Curr. Biol.* 25:3239–3244. https://doi.org/10.1016/j.cub.2015.10.028
Takayama, H., and M.V. Sitkovsky. 1987. Antigen receptor-regulated exocytosis in cytotoxic T lymphocytes. *J. Exp. Med.* 166:725–743. https://doi.org/10.1084/jem.166.3.725
Tamzalit, F., D. Tran, W. Jin, V. Boyko, H. Bazzi, A. Kepecs, L.C. Kam, K.V. Anderson, and M. Huse. 2020. Centrioles control the capacity, but not the specificity, of cytotoxic T cell killing. *Proc. Natl. Acad. Sci. USA.* 117:4310–4319. https://doi.org/10.1073/pnas.1913220117
Wickham, H. 2009. ggplot2: Elegant graphics for data analysis. Springer, New York. https://doi.org/10.1007/978-0-387-98141-3
Wülfing, C., J.D. Rabinowitz, C. Beeson, M.D. Sjaastad, H.M. McConnell, and M.M. Davis. 1997. Kinetics and extent of T cell activation as measured with the calcium signal. *J. Exp. Med.* 185:1815–1825. https://doi.org/10.1084/jem.185.10.1815
Xia, F., C.R. Qian, Z. Xun, Y. Hamon, A.M. Sartre, A. Formisano, S. Mailfert, M.C. Phelipot, C. Billaudeau, S. Jaeger, et al. 2018. TCR and CD28 Concomitant Stimulation Elicits a Distinctive Calcium Response in Naive T Cells. *Front. Immunol.* 9:2864. https://doi.org/10.3389/fimmu.2018.02864
Yachi, P.P., J. Ampudia, T. Zal, and N.R. Gascoigne. 2006. Altered peptide ligands induce delayed CD8-T cell receptor interaction--a role for CD8 in distinguishing antigen quality. *Immunity.* 25:203–211. https://doi.org/10.1016/j.immuni.2006.05.015
Yeung, T., G.E. Gilbert, J. Shi, J. Silvius, A. Kapus, and S. Grinstein. 2008. Membrane phosphatidylserine regulates surface charge and protein localization. *Science.* 319:210–213. https://doi.org/10.1126/science.1152066
Yi, J., X. Wu, A.H. Chung, J.K. Chen, T.M. Kapoor, and J.A. Hammer. 2013. Centrosome repositioning in T cells is biphasic and driven by microtubule end-on capture-shrinkage. *J. Cell Biol.* 202:779–792. https://doi.org/10.1083/jcb.201301004
Zahm, C.D., V.T. Colluru, and D.G. McNeel. 2017. Vaccination with High-Affinity Epitopes Impairs Antitumor Efficacy by Increasing PD-1 Expression on CD8+ T Cells. *Cancer Immunol. Res.* 5:630–641. https://doi.org/10.1158/2326-6066.CIR-16-0374
Zehn, D., S.Y. Lee, and M.J. Bevan. 2009. Complete but curtailed T-cell response to very low-affinity antigen. *Nature.* 458:211–214. https://doi.org/10.1038/nature07657
Zehn, D., S. Roepke, K. Weakly, M.J. Bevan, and M. Prlic. 2014. Inflammation and TCR signal strength determine the breadth of the T cell response in a bim-dependent manner. *J. Immunol.* 192:200–205. https://doi.org/10.4049/jimmunol.1302289
Zhou, X., K.S. Friedmann, H. Lyrmann, Y. Zhou, R. Schoppmeyer, A. Knörck, S. Mang, C. Hoxha, A. Angenendt, C.S. Backes, et al. 2018. A calcium optimum for cytotoxic T lymphocyte and natural killer cell cytotoxicity. *J. Physiol.* 596:2681–2698. https://doi.org/10.1113/JP274964

JCB

Supplemental material

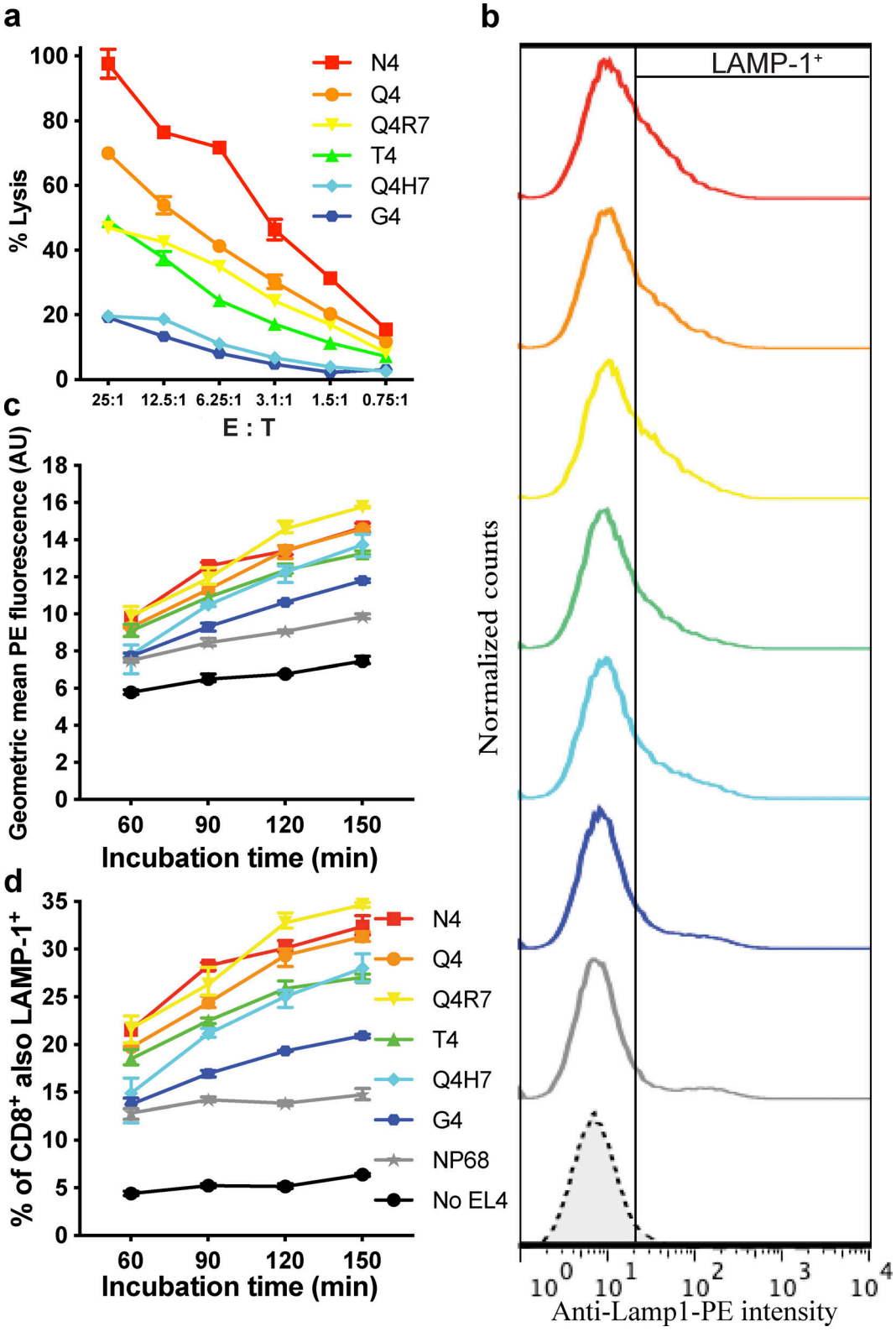

Figure S1. **Stronger TCR signal strengths increase CTL killing efficiency. (a)** Killing assay with OTI CTLs incubated with EL4 pulsed with APL as shown at the CTL effector to target (E:T) ratios shown. Target lysis measured by LDH release, showing mean ± SD of triplicate values for one representative experiment of six. **(b)** LAMP-1 degranulation assay, showing LAMP-1 signal from OTI CTLs (gated on CD8) incubated with EL4 pulsed with APL (indicated by same colors as in [a]) or no EL4 (broken line) for 2.5 h. **(c and d)** Geometric mean fluorescence (c) and percentage LAMP1+ CTL against time (d) showing means of triplicate samples ± SD from one representative experiment of two.

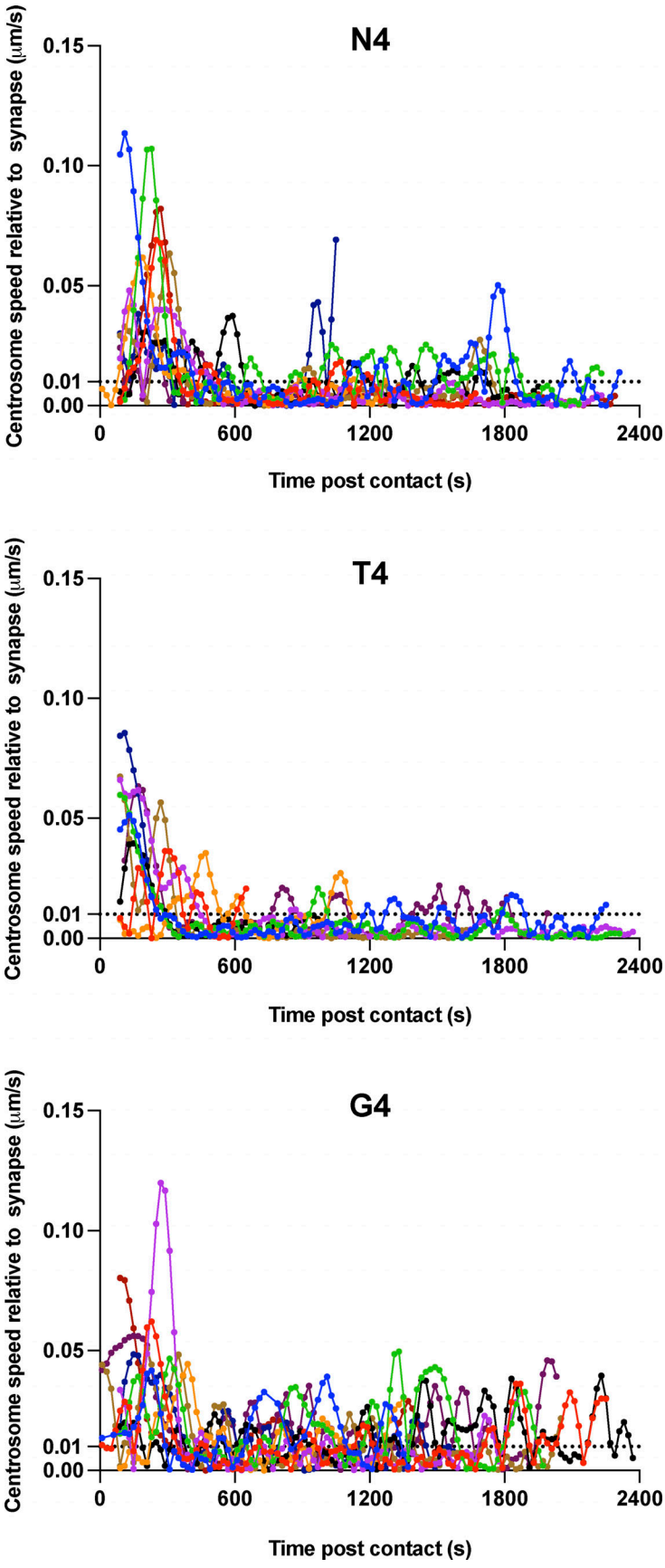

Figure S2. **Centrosome speed is unaffected by TCR signal strength.** Related to Fig. 3 b. Segmented centrosome speed relative to the synapse measured across the duration of the interaction for *n* = 10 (N4 and G4) or *n* = 9 (T4) independent CTL–target interactions, with each color representing a different CTL.

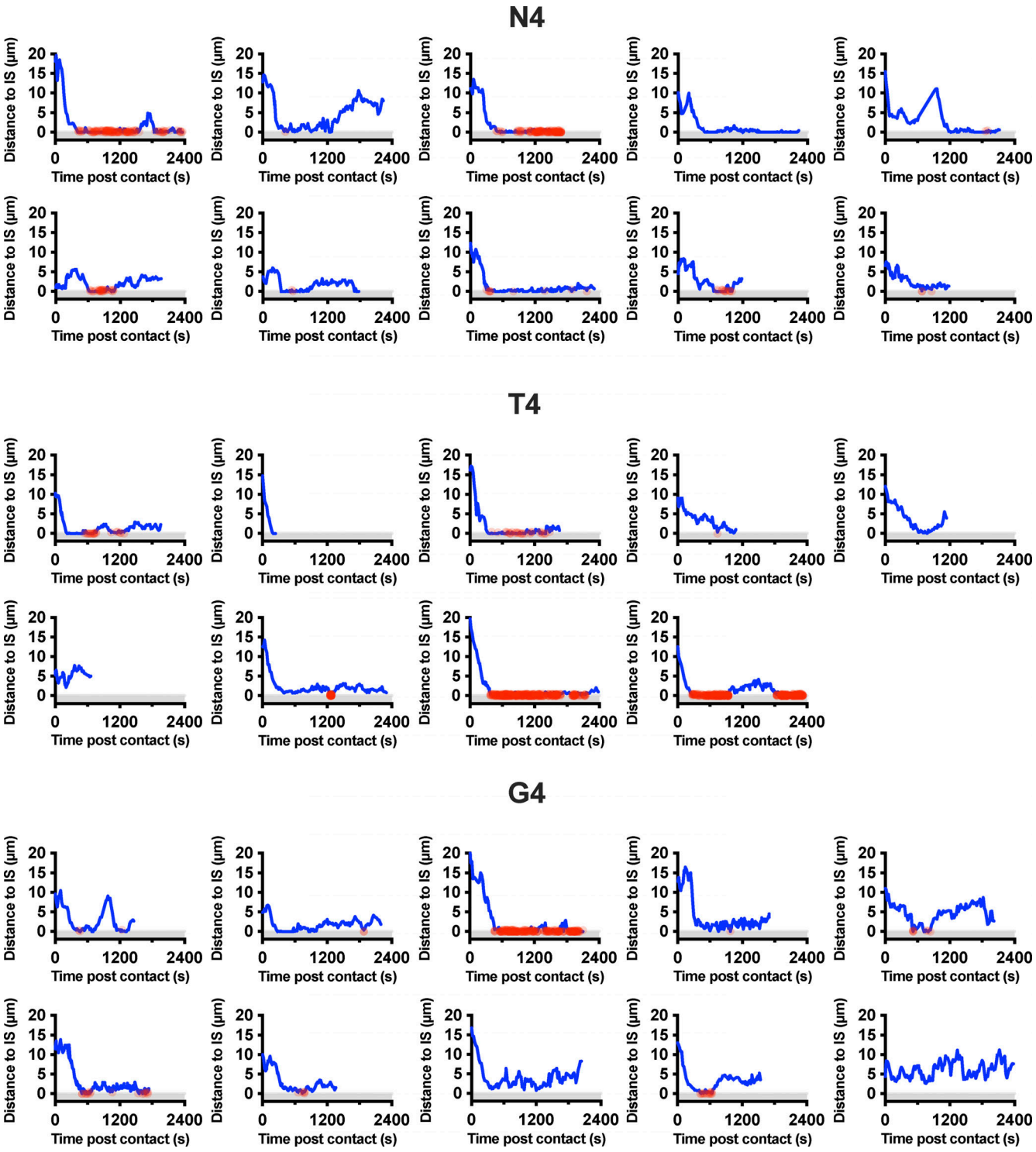

Figure S3. **Centrosome and granule docking.** Related to Fig. 4, g–l. GzmB-TdTomato OTI CTLs expressing Lifeact-EGFP and BFP-PACT interacting with EL4, pulsed with N4, T4, or G4 peptides, were segmented using Imaris to measure relative distances to the synapse. R was used to filter granules for concomitant centrosome docking and granule delivery (<0.5 µm of the synapse). Red spots show granules reaching the synapse on blue lines showing centrosome distance from the synapse, from total CTL of N4 = 10, T4 = 9, and G4 = 10. Representatives were taken from these for Fig. 4, g–l.

Video 1. **Increasing TCR signal strength increases CTL dwell time.** Related to Fig. 1 a. OTI CTLs expressing Lifeact-mApple (green) and RFP-PACT (green) interacting with EL4 (blue), pulsed with N4, G4, or NP68 peptides. APL relates to the maximum-intensity projection representative time series of OTI CTLs encountering targets shown in Fig. 1. Scale bars = 5 µm; time min:s from start of recording. Playback speed, 10 frames per second.

Video 2. **Increasing TCR signal strength increases centrosome docking at the synapse.** Related to Fig. 3 a. GzmB-TdTomato (red) OTI CTLs expressing Lifeact-EGFP (green) and BFP-PACT (white sphere) interacting with EL4 (blue), pulsed with N4, T4, or G4 peptides. APL relates to the representative time series maximum-intensity projection of OTI CTLs encountering targets shown in Fig. 3 a. Scale bars = 5 µm; time min:s from start of recording. Playback speed, 10 frames per second.

Video 3. **Prolonged docking of the centrosome to the synapse promotes granule delivery to the synapse.** Related to Fig. 4, a–c. GzmB-TdTomato (red) OTI CTLs expressing Lifeact-mApple (green) and BFP-PACT (white sphere) interacting with EL4-blue, pulsed with N4, T4, or G4 peptides. APL relates to the representative maximum-intensity projection time series of OTI CTLs encountering targets shown in Fig. 4, a–c. Scale bars = 5 µm; time min:s from start of recording. Playback speed, 10 frames per second.

Video 4. **Calcium flux precedes centrosome polarization and uropod retraction.** Related to Fig. 5 a. OTI CTLs expressing GCAMP6m (green), Lifeact-mApple (red), and RFP-PACT (red sphere) interacting with EL4 (blue), pulsed with N4. Video relates to representative maximum-intensity projection time series of OTI CTLs encountering N4 pulsed target in Fig. 5 a. Scale bars = 5 µm; time min:s after start of recording. Playback speed, 10 frames per second.

Video 5. **Duration of initial calcium fluxes are increased with higher-affinity ligands.** Related to Fig. 6 a. OTI CTLs expressing GCAMP6m (green), Lifeact-mApple (red), and RFP-PACT (red sphere) interacting with EL4 (blue), pulsed with N4, T4, or G4. Representative maximum-intensity projection time series of OTI CTLs encountering APL pulsed targets. Scale bars = 5 µm; time min:s from start of recording. Playback speed, 10 frames per second.